

Treatment of chromium effluent by adsorption on chitosan activated with ionic liquids

Key Pontes Eliodorio · Vitor Seorra Andolfatto · Marco Rulevas Gomes Martins · Breno Pivaro de Sá · Erick Ryoiti Umeki · Andreia de Araújo Morandim-Giannetti

Received: 12 July 2016 / Accepted: 20 March 2017 / Published online: 22 March 2017
© Springer Science+Business Media Dordrecht 2017

Abstract This study proposes, verifies, and refines the use of biopolymers treated with two new ionic liquids (ILs) (*sec*-butylammonium acetate and *n*-octylammonium acetate), as a platform for chromium adsorption. The ILs were synthesized, characterized, and applied to chitosan treatment. Analyzing the size distribution of microparticles of chitosan and chitosan activated with ILs (*sec*-butylammonium acetate and *n*-octylammonium acetate), we observed that a little decrease in the particle size occurred with the activation of chitosan ($176 \pm 0.02 \mu\text{m}$ to 167 ± 0.054 and $168.5 \pm 0.05 \mu\text{m}$, respectively), as well as changes in the X-ray diffraction FTIR_ATR spectra. Further studies were performed using the best adsorbent – chitosan treated with *sec*-butylammonium acetate. In this case, the chromium VI concentration in the sample was reduced by more than 99% when using chitosan treated with IL *sec*-butylammonium acetate. The best reaction time was determined as 1 h, which allowed a

chromium adsorption of 99.1% and the adsorption kinetic data were best represented by the second-order model ($k_2 = 11.7258 \text{ g mg}^{-1} \text{ min}^{-1}$). The maximum adsorption capacity was obtained using the Langmuir isotherm model (20.833 mg g^{-1} at pH 4 during 1 h, using 1.0 g of chitosan), and the adsorption efficiency was enhanced at 25 °C by the Freundlich isotherm model, in which the constants KF and n were determined as 0.875 mg L^{-1} and 1.610, respectively.

Keywords Wastewater treatment · Hexavalent chromium · Chitosan · Ionic liquids

Introduction

Water is fundamental to life and its preservation becomes fundamental to maintaining the balance of the ecosystem, especially after rapid industrialization has released excessive amounts of heavy metals into the environment through industrial wastewaters (Gupta et al. 2012a). The removal of these contaminants until acceptable limits becomes necessary, as they are not degradable and the accumulation of these metals in the nature may lead to serious health issues (Saleh and Gupta 2014; Gupta et al. 2012b). These contaminants are released by a range of industries, including plastic, pigment, wood preservative, electroplating, leather tanning, cement, mining, dyeing, refractory materials, catalysis, fertilizer industries and

Electronic supplementary material The online version of this article (doi:10.1007/s10570-017-1264-3) contains supplementary material, which is available to authorized users.

K. P. Eliodorio · V. S. Andolfatto · M. R. G. Martins · B. P. de Sá · E. R. Umeki · A. de Araújo Morandim-Giannetti (✉)
Department of Chemical Engineering, Centro Universitário FEI, Av. Humberto de Alencar Castelo Branco, 3972, São Bernardo do Campo, SP 09850-901, Brazil
e-mail: preamorandim@fei.edu.br

can cause serious environmental problems as aesthetic pollution, eutrophication and perturbations to aquatic life (Gore et al. 2016; Xiang et al. 2016; Zhou et al. 2016; Saleh and Gupta 2014; Mittal et al. 2009a; Gupta et al. 2011a).

Of these contaminants, heavy metals ions such as chromium ions, especially hexavalent chromium, are highly toxic to aquatic animals and humans and can cause severe diseases such as dermatitis, kidney failure, liver and gastric damage, lung cancer, mutagenesis, and even death (Gore et al. 2016; Kahu et al. 2016; Zhou et al. 2016; Gupta et al. 2015; Tan et al. 2015).

For this reason, HCrO_4^- or $\text{Cr}_2\text{O}_7^{2-}$ is considered an extremely hazardous pollutant; reducing its concentration within the tolerance recommended by the World Health Organization (WHO) has been extensively researched. The recommended limit is 0.10 mg/L in effluents (Gore et al. 2016; Kahu et al. 2016; Zhou et al. 2016; Kumar et al. 2012).

For this purpose, we have investigated various mechanical, physicochemical, and biological treatments based on cation surfactant and adsorption, which are lauded for their high efficiency and flexibility, low cost, separation and simplicity of design and operation (Gomes et al. 2016; Gore et al. 2016; Xiao et al. 2016; Zhou et al. 2016; Borsagli et al. 2015; Gupta and Nayak 2012; Mittal et al. 2009b; Saleh and Gupta 2012a; Gupta et al. 2012c, 2015).

Among these treatments, we can find chemical precipitation, ion exchange, membrane processes, electrodialysis, reverse osmosis, photocatalytic degradation, coagulation, flocculation, oxidation/reduction, sedimentation, filtration, solvent extraction and adsorption. These treatments are being classified as primary water treatment technologies, secondary water treatment technologies and tertiary water treatment technologies (Gomes et al. 2016; Xiao et al. 2016; Borsagli et al. 2015; Gupta et al. 2012a, 2015; Luo et al. 2015; Matouq et al. 2015; Zeng et al. 2015; Saleh and Gupta 2014; Gupta and Saleh 2013; Karthikeyan et al. 2012; Mittal et al. 2009b).

Of these, adsorption occurs because surface atoms have unbalanced attractive forces, such as hydrogen bonds, dipole–dipole interactions and ion–dipole interactions. To compensate for these attractive forces, the solid phase adsorbs the molecules present in the fluid phase. These interactions can be potentiated by chemically treating the adsorbent matrix (Gomes et al. 2016; Kumar et al. 2012).

However, most of the investigated adsorbents and biosorbents have been studied and used for decades (Gupta et al. 1997), such as granular activated carbon, active diatomaceous earth, iron oxide, polysaccharides, resins, biomaterials, nanocomposites, carbon nanotubes, activated sludge, graphene oxide, L-cysteine functionalized Fe_3O_4 magnetic nanoparticles, Fe_3O_4 nanoparticles functionalized and stabilized with compounds like humic acid, castor seed shell, sugar industry waste material, alumina, kaolinite, lignocellulosic materials and extracellular polymeric substances. One possible problem when using an adsorbent is an agglomeration of particles during its first use. Attempts to minimize this effect, which reduces the adsorbent reuse efficiency, have been published (Gore et al. 2016; Fan et al. 2016; Gupta et al. 2015, 2013, Gupta et al. 2011b; Ma et al. 2015; Malekia et al. 2015; Yue et al. 2015; Gupta and Saleh 2013; Gupta and Nayak 2012; Karthikeyan et al. 2012; Saleh and Gupta 2012b; Mittal et al. 2010a, b).

Furthermore, the preferred adsorbents should possess high surface area. Additionally, their nano-sized shapes may increase efficiency during the adsorption process. In this case, the high cost to produce nanoparticles is a problem (Gore et al. 2016; Malekia et al. 2015; Polowczyk et al. 2016; Xiao et al. 2015).

Therefore, new techniques that improve the efficiency of adsorption are highly demanded. Efficient heavy-metal absorbers include polysaccharides such as chitosan (prepared by chitin deacetylation) and lignocellulosic materials (comprising cellulose, hemicelluloses, and lignin, or starch and derivatives) (Gomes et al. 2016; Gore et al. 2016; He et al. 2016; Jia et al. 2016; Wu et al. 2016; Li et al. 2015; Malekia et al. 2015; Zeng et al. 2015).

Chitosan is an excellent choice for an adsorbent, as it is biodegradable, non-toxic, abundantly available, chemically stable, highly reactive, in addition to having excellent chelation properties and a low cost. Its adsorptive capacity is related to the large numbers of primary amine and hydroxyl groups in the chitosan chain, which can serve as coordination and reaction sites. The adsorption capacity can be further enhanced by chemical treatments with ionic liquids, cross-linking processes, and composite production (He et al. 2016; Kahu et al. 2016; Yang et al. 2016; Shinde et al. 2013; Jeon and Holl 2003; Kumar et al. 2012).

However, the adsorption of heavy metals is affected by multiple factors, including temperature, pH, metal

concentration, and type of adsorbent material. Each of these factors can modify the manner wherein a metal ion finds and remains on an active site on the adsorbent. Therefore, to maximize the adsorbent utilization and metal ion removal, we must optimize the values of these parameters (Kahu et al. 2016; Gupta et al. 2015; Kumar et al. 2012).

In this context, we analyzed the effects of pH, contact time, and initial concentration of the adsorption capacities of Cr(VI) on chitosan. To this end, we treated chitosan with the ionic liquid (IL) *sec*-butylammonium acetate and determined the equilibrium adsorption isotherms of Cr(VI) on this material by the Langmuir and Freundlich equations and adsorption kinetic.

Materials and methods

Materials

To prepare the required solutions or ILs, we purchased the following analytical grade reagents: *sec*-butylamine (99.0%) and *n*-octylamine (99.0%), methanol (99.9%), ethanol (99.5%), potassium dichromate (99.0%), acetic acid (99.5%) and Chloroform-*d* (≥ 99.96 atom % D) from Sigma-Aldrich (St. Louis, MO, USA). Chitosan (degree of de-acetylation of 86.7%, 80 meshes) was purchased from Polymar (Fortaleza, CE, Brazil).

Experimental

IL synthesis

The ILs were obtained by the acid–base neutralization reaction. The acetic acid was slowly added to an aliphatic amine (*sec*-butylamine or *n*-octylamine) under stirring. The obtained ILs were *n*-octylammonium acetate (1), unprecedented in the literature, and *sec*-butylammonium acetate (2) (Andrade Neto et al. 2016; Dyson et al. 1999).

The stoichiometric ratio was 1:1. The reaction temperature was maintained between 20 and 40 °C. After 2 h of acid addition, the IL products were stirred for a further 60 min and maintained for 48 h in an amber bottle. After the incubation period, the ILs were characterized by nuclear magnetic resonance (NMR) and infrared (IR) spectrometry. The ^1H and ^{13}C NMR

spectra were obtained in Chloroform-*d* (CDCl_3) with a Bruker Avance III 600 HD spectrometer operating at 600 MHz for protons and 150 MHz for carbon.

Chemical shifts (δ , ppm) were reported relative to tetramethylsilane (TMS). The IR spectra were obtained by Fourier transform IR spectroscopy (Nicolet 6700) with attenuated total reflectance (FTIR–ATR). The scanning conditions were 32 scans per spectrum at a spectral resolution of 4 cm^{-1} in the wavenumber range of $4000\text{--}450\text{ cm}^{-1}$.

Attributions of signals to hydrogens and carbons were assisted by the COSY technique (Homomuclear Correlation Spectroscopy), HSQC (Heteronuclear Single Quantum Coherence) and HMBC (Heteronuclear Multiple Bond Coherence). These techniques analyze the correlations between neighboring hydrogens and between neighboring or adjacent hydrogens and carbons in bidirectional spectra.

Treatment of chitosan

During the IL-treatment of chitosan, 1.00 g of the IL (*n*-octylammonium acetate or *sec*-butylammonium acetate) was dissolved in 30 mL of methanol or ethanol. 12 g of chitosan were placed into a round-bottomed flask and the dissolved ionic liquid was added dropwise and sonicated by ultrasound (UltraCleaner, model USC 1600 A, UNIQUE; Brazil) for 2 h with an intermittent time interval of 15 min (Kumar et al. 2012).

The resulting solution was filtered and washed with methanol or ethanol. The filtrate was dried at room temperature and retained for further adsorption studies. The effective impregnation of the IL by ultrasonication was ascertained through a comprehensive physicochemical characterization of the adsorbent material.

Characterization of chitosan

The pure chitosan and chitosan activated with *n*-octylammonium acetate or *sec*-butylammonium acetate were submitted for analysis of the granulometric distribution of the microparticles, as well as analysis through infrared spectroscopy and X-ray diffraction.

The granulometric distribution of the microparticles of chitosan before and after activation was performed by laser diffraction using a Laser Particle Size Analyzer Microtrac Bluewave (Montgomeryville, USA), which measures particle sizes from 0.01 to 2800 microns. The

microparticles were analyzed in dry mode in triplicate and their size distribution was determined.

The infrared spectroscopy analyses were performed using a Thermo Scientific Nicolet 6700 FT-IR spectrophotometer (Madison, USA). The attenuated total reflectance spectra were collected in the range of 4000–500 cm^{-1} with a resolution of 2 cm^{-1} and 32 scans per sample.

An X-ray diffraction (XRD) analysis was performed on an X-ray diffractometer (XRD-7000 Model, Shimadzu). The operating voltage and current were maintained at 40 kV and 35 mA, respectively, and the angular range was 3–135°. The diffraction spectra were collected using the θ – 2θ method. The samples were scanned in the 2θ range 5–40° in steps of 0.015°. The radiation (Cu K α X-ray source) wavelength was 1.5406 Å. The degree of crystallinity (X_c) was calculated as the area under the crystalline peaks relative to that of the non-crystalline region (Eq. 1).

$$X_c = \frac{F_c}{F_a + F_c} \times 100 \quad (1)$$

where F_c and F_a denote the areas under the crystalline and non-crystalline regions, respectively.

Adsorption procedure using batch method

Before analyzing the optimal conditions for chromium (VI) adsorption to the IL-treated chitosan, we determined the IL that best interacted with chitosan and yielded the best activation of the adsorbent.

In this evaluation, a 25.00 mL chromium (VI) solution (45.00 mg L^{-1}) was placed in contact with 1.00 g of adsorbent (chitosan treated with *n*-octylammonium acetate or *sec*-butylammonium acetate in the presence of methanol or ethanol) in an orbital incubator shaker (Inova 43, Eppendorf International; Germany) at room temperature. The samples were filtered and the percentage of adsorbed chrome VI was determined through plasma emission spectroscopy using a plasma spectroscope (ICPE-9000 model, Shimadzu, Japan). The relative concentrations of adsorbed chromium VI were expressed as percentages.

After checking the favorable IL for chitosan activation (*sec*-butylammonium acetate), this adsorbent condition was optimized in a series of experiments. For this, studies of ideal pH and time were performed, as well as the adsorption isotherm and kinetics studies. First, we checked the influence of pH

on chromium adsorption to the same absorbent. In this experiment, the pH varied from 2 to 4.5. The pH values of the solutions were adjusted by adding H_2SO_4 solution (0.1 mol L^{-1}) or NaOH solution (0.1 mol L^{-1}). To perform the studies concerning the optimum adsorption time, experiments were carried out using adsorption times which varied from 10 to 600 min. All concentrations were determined by plasma emission spectroscopy.

Adsorption kinetics

The study of hexavalent chromium adsorption dynamics describes the rate of solute uptake, and it depends on the chemical and physical characteristics of the adsorbent material as well as the mass transfer, which controls the residence time of adsorbate uptake at the solid–solution interface. In order to establish the kinetics of hexavalent chromium adsorption, the adsorption dynamics of the chitosan treated with IL *sec*-butylammonium acetate was investigated by using the kinetic model of pseudo-first-order Eq. (2) and the pseudo-second order Eq. (3), using reaction times which varied from 10 to 600 min.

$$\log(q_e - q_t) = \log q_e - \frac{k_1 t}{2.303} \quad (2)$$

$$\frac{t}{q_t} = \frac{1}{k_2 q_e^2} + \frac{t}{q_e} \quad (3)$$

where q_t is the concentration of Cr(VI) (mg/g of adsorbent) removed at time t (min), q_e is the concentration of Cr(VI) removed at equilibrium time, and k_1 and k_2 are the rate of pseudo-first-order rate constant of adsorption (min^{-1}) and the rate of pseudo-second-order rate constant of adsorption (g/mg/min), respectively.

Isotherm acquisition

Having confirmed the best adsorbent (*sec*-butylammonium acetate) and optimized the pH and time of adsorption, we prepared seven chromium solutions with different concentrations (50–500 ppm). Twenty-five milliliters of each solution (pH = 4.0) were added to a 250 mL Erlenmeyer flask, along with 1.00 g of chitosan treated with *sec*-butylammonium acetate prepared in the presence of methanol. The samples were placed on a shaker for 1.0 h with stirring at various temperatures (20, 25, 30, and 35 °C).

The samples were filtered and the obtained filtrates were characterized by plasma emission spectroscopy. The amount of chromium adsorbed (mg g^{-1}) at equilibrium (q_e) is calculated by Eq. (4)

$$q_e = \frac{(C_0 - C_e) \times V}{W} \quad (4)$$

where C_0 and C_e are the initial and final concentrations (mg L^{-1}) of chromium(VI), respectively, V is the volume (L) of aqueous chromium solution, and W is the weight (g) of the ionic liquid impregnated with the chitosan adsorbent used in the batch adsorption study.

The Langmuir and Freundlich isotherms were then obtained according to Eqs. 4 and 5, respectively:

$$\frac{C_e}{q_e} = \frac{1}{q_0 b} + \frac{C_e}{q_0} \quad (5)$$

where q_e is the mass of solute adsorbed per gram of adsorbent (g/g or mg/g), C_e is the final chromium(VI) concentration (mg L^{-1}), q_0 is the maximum adsorption capacity, and b is a constant obtained from the slope and intercept of the C_e/q_e versus C_e plot. In Eq. (6)

$$\log q_e = \log K_f + \frac{1}{n} \log C_e \quad (6)$$

where q_e is the mass of solute adsorbed per gram of adsorbent (g/g or mg/g), n and K_f are empirical constants, and C_e is the solute concentration in the solution at equilibrium (mg L^{-1}).

The adsorption efficiency was expressed as the dimensionless parameter R_L calculated by Eq. (7). Equation 7 can also be determined from the relation between the empirical constants K_f and $1/n$.

$$R_L = \frac{1}{1 + bC_0} \quad (7)$$

where R_L indicates the effectiveness of the adsorption.

Results and discussion

Synthesis and characterization of ionic liquids

Starting from acetic acid and *sec*-butylamine or *n*-octylamine (Fig. 1), we synthesized two ILs in the laboratory. Both ILs were characterized by hydrogen NMR (^1H NMR), carbon NMR (^{13}C NMR), and FTIR–ATR.

In the spectra of the synthesized ionic liquids (ILs), the amino groups of *n*-octylamine and *sec*-butylamine were chemically displaced after the formation of *n*-octylammonium and *sec*-butylammonium ions. This indicates the protonation of the amino group and the change in the multiplicity of the signal related to amine hydrogens. The integration in amines and ILs was observed by the presence of two and three hydrogen signals, respectively.

The FTIR–ATR data were also altered by amino group protonation, corroborating the results of the NMR analysis, and changes in carbonyl absorption were noted. In particular, the intense carbonyl band around 1700 cm^{-1} shifted to the 1600 cm^{-1} region in the ILs, indicating the carbonyl of carboxylic salts (Pavia et al. 2015; Silverstein et al. 2005).

IL-1: ^1H NMR (600 MHz, CDCl_3): δ 1.93 (3H, s, H-2), 1.24 (3H, d, H-3), 3.04 (1H, m, H-4), 1.54 and 1.70 (2H, m, H-5), 0.96 (3H, t, H-6), 6.08 (3H, s, NH_3^+). ^{13}C NMR (150 MHz, CDCl_3): δ 178.55 (C-1), 28.63 (C-2), 18.85 (C-3), 48.61 (C-4), 24.40 (C-5), 10.22 (C-6). FTIR–ATR (cm^{-1}): ν_{max} 3100–2600, 2200–2000, 1620, 1580.

IL-2: ^1H NMR (600 MHz, CDCl_3): δ 1.91 (3H, s, H-2), 2.77 (2H, t, H-3), 1.60 (2H, m, H-4), 1.27 (10H, m, H-5→H-9), 0.87 (3H, t, H-10), 6.38 (3H, s, NH_3^+). ^{13}C NMR (150 MHz, CDCl_3): δ 178.86 (C-1), 24.51 (C-2), 39.85 (C-3), 29.27 (C-4), 22.75 (C-5), 31.88 (C-6), 2915 (C-7), 28.87 (C-8), 26.80 (C-9), 14.21 (C-10). FTIR–ATR (cm^{-1}): ν_{max} 3100–2500, 2200–2000, 1620, 1580, 1463.

Chitosan treatment

Initially, chitosan was separately treated with *sec*-butylammonium acetate and *n*-octylammonium acetate in the presence of methanol or ethanol. By employing two different solvents, we were able to check the influence of the solvent on the chitosan–IL interaction (Kumar et al. 2012).

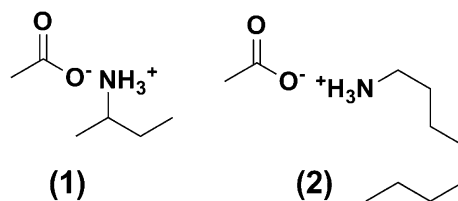


Fig. 1 Ionic liquids obtained by acid–base neutralization

The interaction between chitosan and ILs can be attributed to hydrogen bonds, as evidenced by Kumar et al. (2012). However, to confirm changes in the surface of chitosan after treatment, analyses were performed to determine changes in particle size distribution as well as changes in crystallinity and absorption bands in the infrared region.

Analyzing the size distribution of microparticles of chitosan and chitosan activated with ionic liquids (*sec*-butylammonium acetate and *n*-octylammonium acetate), we observed that the dimensions and granulometric distribution changed.

We also verified that a little decrease in the particle size occurred with the activation of chitosan, from $176 \pm 0020 \mu\text{m}$ to $167 \pm 0,054$ and $168.5 \pm 0,050 \mu\text{m}$, by using the ILs *sec*-butylammonium acetate and *n*-octylammonium acetate, respectively. This probably happens due to the agglomeration of particles, which is facilitated by the interactions between the chitosan and the ILs.

The X-ray diffraction spectra (Fig. 2) revealed an amorphous chitosan in the 2θ range $20\text{--}25^\circ$. This structure is attributed to the intramolecular hydrogen bonds in the chitosan chains. The characteristic peaks of α -chitosan were observed at $2\theta = 10.5, 20.25$ and 22.5° , as evidenced by Ma et al. 2015. After treatment with *sec*-butylammonium acetate in a methanol solvent, the higher value was slightly shifted and its intensity was reduced. These changes were absent in the other tested treatments (chitosan treated with *n*-octylammonium acetate in the presence of methanol or

ethanol, and chitosan treated with *sec*-butylammonium acetate in the presence of ethanol).

The decreased crystallinity of chitosan might be explained by intramolecular hydrogen bonding in the chitosan and by intermolecular hydrogen bonding between *sec*-butylammonium cations and the chitosan chains (Kumar et al. 2012). This analysis consolidates the more effective interaction of chitosan with *sec*-butylammonium acetate compared to *n*-octylammonium. The large size of the latter ions probably increases the steric obstruction, hampering the interaction between the chitosan and the IL (Table 1).

The interaction between chitosan and *sec*-butylammonium acetate generates changes in the region between 18 and 23° due to the interaction of ionic liquid with the hydroxyls present in the chitosan, which can be confirmed by the reduction of the band referring to the O–H binding after the analysis via FTIR-ATR (Kahu et al. 2016).

Finally, the FTIR spectral analysis (Fig. 3) showed characteristic bands referring to a strong absorption band at 3354 cm^{-1} due to O–H and amine N–H symmetrical stretching vibrations, which decreases after activation with IL because of the interaction between the NH_3^+ group of the ionic liquid and the hydroxyl groups of chitosan (Silverstein et al. 2005). It is also possible to observe a peak at 2923 and 1070 cm^{-1} attributed to C–H and the C–O stretching, respectively. The N–H bending vibration at 1583 cm^{-1} is shifted to 1561 cm^{-1} after the impregnation with the ionic liquid. Similarly, the C–N bending vibration observed at 1375 cm^{-1} resulted in a shift to 1312 cm^{-1} . These changes could be attributed to the effective interaction of the *sec*-butylammonium or *n*-octylammonium cations with the hydroxyl group of chitosan in the form of an intermolecular hydrogen bonding interaction. Indeed, the interaction of ammonium cation through hydrogen bonding interaction is an interesting phenomenon

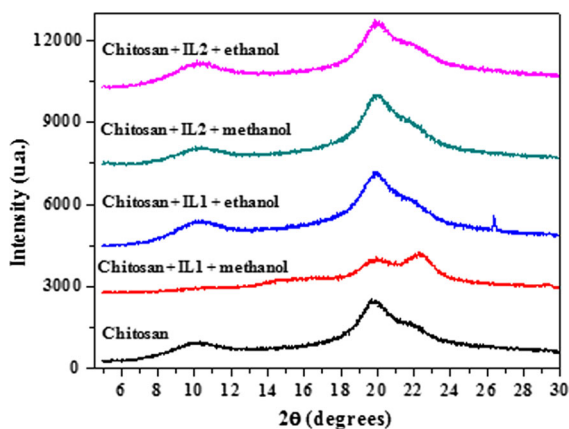


Fig. 2 X-ray diffractograms of chitosan treated with *n*-octylammonium acetate and *sec*-butylammonium acetate in methanol and ethanol solvents

Table 1 Degree of crystallinity of the adsorbents

Adsorbents	Degree of crystallinity (%)
Chitosan	36.95
Chitosan + IL1 + Methanol	33.18
Chitosan + IL1 + Ethanol	36.59
Chitosan + IL2 + Methanol	35.89
Chitosan + IL2 + Ethanol	36.79

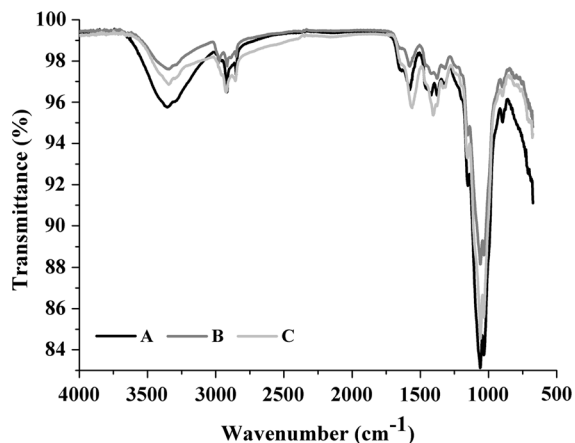


Fig. 3 FTIR spectra of Pure and activated with ILs chitosan: *A* Chitosan; *B* Chitosan + IL1 + methanol; *C* Chitosan + IL2 + methanol

observed in host–guest interaction, as highlighted by Kumar et al. (2012).

Chromium adsorption

Based on the initial analysis of the obtained adsorbents, we analyzed the chromium adsorption of the four prepared materials (*sec*-butylammonium acetate and *n*-octylammonium acetate in the presence of methanol and ethanol). In this analysis, we have confirmed the most efficient treatment of chitosan with *sec*-butylammonium acetate in methanol solvent. To this end, we compared the chromium adsorption rates of the various adsorbents. 1 g of adsorbent was exposed to 25.00 mL of chromium solution at an initial concentration of 45 mg L⁻¹ (Fig. 4).

A final concentration of chromium of 0.21 ppm was observed when the chitosan activated with the *sec*-butylammonium acetate was used. The lowest efficiency was also observed when the *n*-octylammonium acetate or chitosan were used (14.00 and 6.12 ppm, respectively). It was also verified that *n*-octylammonium acetate IL inhibits the adsorption process of the chromium ion, due to its very long chain. The adsorption effectiveness is presented as a percentage of chromium ion adsorbed (Fig. 4).

Having confirmed the best adsorbent as chitosan treated with *sec*-butylammonium acetate in the presence of methanol, we analyzed the influence of the preparation parameters; namely, the adsorbent mass, solution pH, and the adsorption time and temperature of this adsorbent.

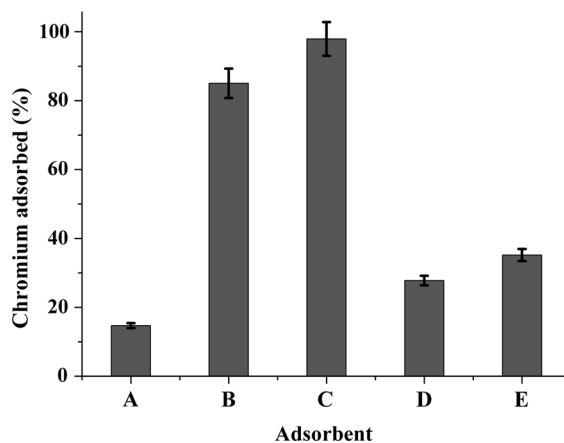


Fig. 4 Chromium adsorbed (%) by chitosan treated with various ionic liquids in different solvents: *A* Chitosan; *B* Chitosan *sec*-butylammonium acetate + ethanol; *C* Chitosan *sec*-butylammonium acetate + methanol; *D* Chitosan *n*-octylammonium acetate + ethanol; *E* Chitosan *n*-octylammonium acetate + methanol

Specifically, we aimed to optimize the adsorption conditions for chitosan treated with *sec*-butylammonium acetate, considered the best adsorbent during previous analyses. First, we determined the ideal adsorbent mass in the adsorption experiments.

According to this analysis, chromium VI adsorption was enhanced at 1.00 g of adsorbent; the adsorption was not significantly improved at other masses. Therefore, when analyzing the remaining parameters, we treated 1.00 g of chitosan with *sec*-butylammonium acetate in methanol. Adsorption was also more effective at 20 and 25 °C than at other temperatures. This can be explained by the exothermic adsorption process, which is disadvantaged at a higher temperature (Kumar et al. 2012).

Next, we optimized the pH for chromium VI adsorption. When analyzing the influence of the pH solution on chromium VI adsorption, we should consider the relevant ionic species, as shown in Fig. 5 (Kumar et al. 2012).

Quantitatively, the chromium adsorption was maximized in the pH range of 2.0–4.5. Here, we referred to the characteristics reported by Kumar (2012). In this pH range, the active binding sites in *sec*-butylammonium acetate and chitosan interact with the hexavalent hydrogen chromate oxy anion, favoring the adsorption of chromium VI.

The percentage of chromium adsorption declines after pH 4.0 because the surface amino group deprotonates; subsequently, hydroxide ions compete for the

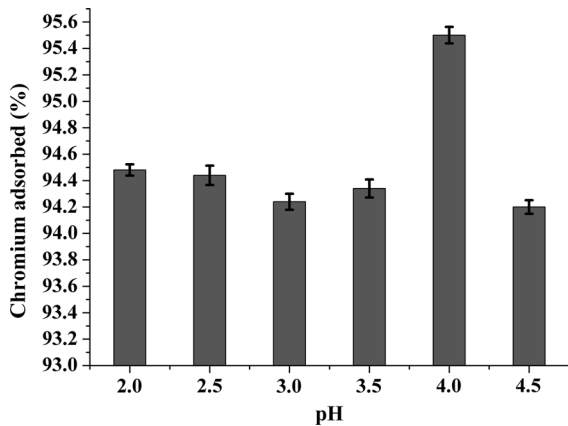


Fig. 5 Influence of pH on chromium adsorption

active adsorption sites (Fig. 6). The *sec*-butylammonium cation interacts with the chitosan through hydrogen bonding, followed by electrostatic interaction between the hydrochromate anions and the protonated amine groups in the chitosan.

The uptake of chromium ion by the adsorbent depends on the contact time and in this context, the study of the kinetics of adsorption is of considerable significance. Therefore, in this study, two models were analyzed: the pseudo-first order and second order kinetic models.

This way, we used a ratio between the chromium solution concentrations, before and after the adsorption treatment, in order to determine the quantity of chromium adsorbed in the given period of time. From the data obtained, it was possible to verify that the maximum adsorption happened in 1 h (60 min), with an absorbed quantity of $2.756 \text{ mg g}^{-1} \pm 0.046$, which corresponds to $99.91 \pm 0.08\%$ of adsorption (Fig. 7).

By studying the kinetics of absorption and analyzing the correlation coefficients (R^2), it is noted that the pseudo-second order equation has a better adjustment, representing the kinetic model of the reaction of absorption of chromium in the chitosan activated with ionic liquids (*sec*-butylammonium acetate). Besides, the experimental quantity absorbed (q_e) was similar to the one calculated based on the equational data (q_c) obtained by the pseudo-second order model (Table 2).

To determine the adsorption temperature, we obtained the isotherms and the maximum adsorption capacity that attains the Langmuir isotherm. For the maximum concentration of chromium VI on the adsorbent, we obtained the adsorption capacity and intensity by constructing Freundlich isotherms (Fig. 8).

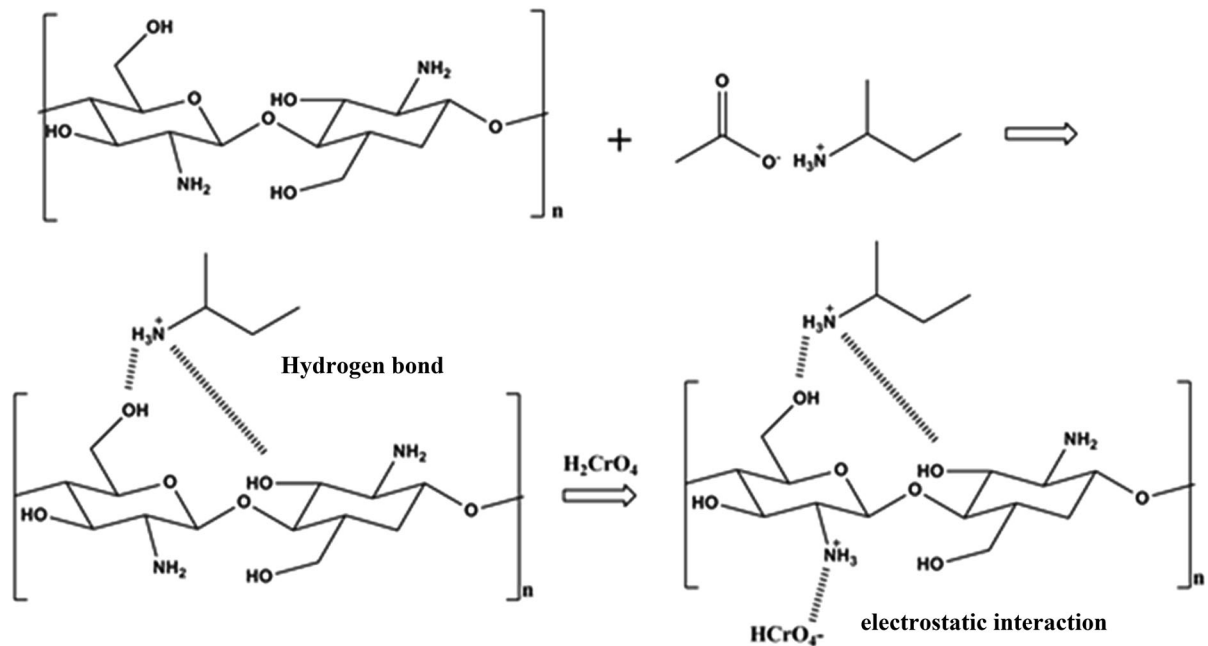


Fig. 6 Interaction between chitosan, the IL *sec*-butylammonium acetate, and the adsorbed chromium

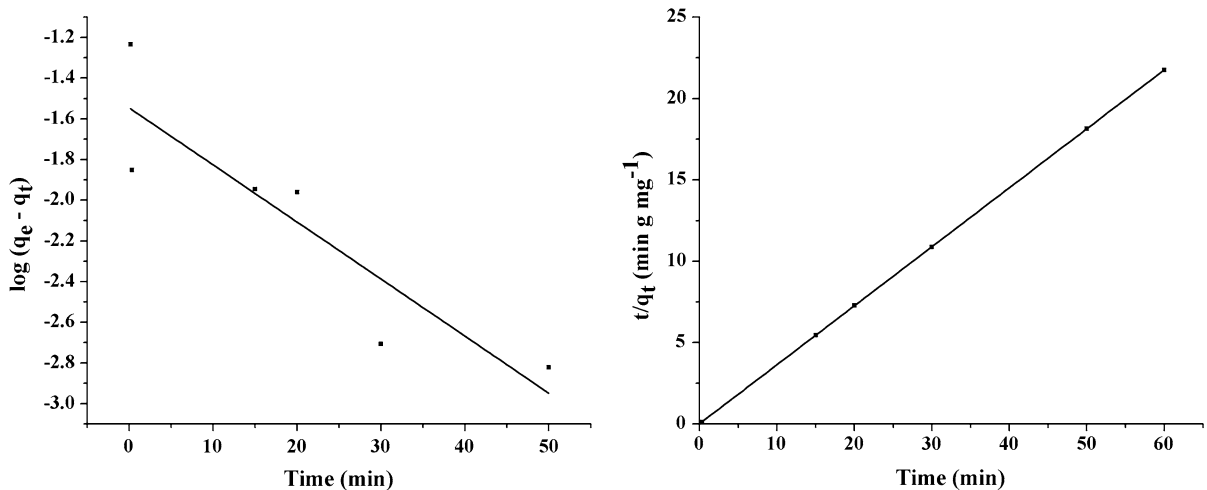


Fig. 7 Kinetic plot for adsorption of chromium ion on activated with ionic liquids

Table 2 Kinetic constant data for the adsorption of chromium (VI)

Model	q_e (mg g^{-1})	q_e calculated (mg g^{-1})	K	R^2
Second order rate constant	2.7580	2.7580	$11.7258 (\text{g mg}^{-1} \text{min}^{-1})$	1.0000
First order rate constant	2.7580	0.0280	$0.0647 (\text{min}^{-1})$	0.7645

By analyzing the Langmuir isotherms at 20, 25, 30, and 35 °C (Fig. 8), we identified the maximum adsorption capacity as 20.833 mg g^{-1} (0.0217 L mg^{-1} ; see Table 3) at 20 °C. The regression coefficient of the relationship was 0.982. Therefore, 20 °C was confirmed as the best working temperature. However, very similar

values were obtained at 25 °C, especially the R_L , which was 0.454 at 20 °C and 0.411 at 25 °C, suggesting that the optimal temperature could reduce the large-scale implementation costs of this IL adsorbent.

The R_L values are very similar to those reported by other authors, demonstrating the efficiency of the

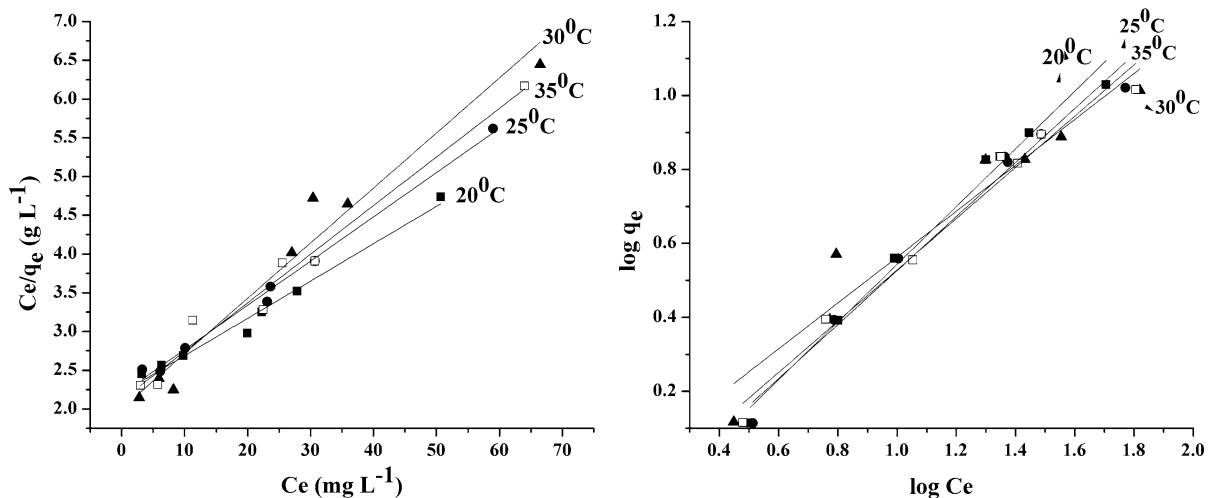


Fig. 8 Langmuir and Freundlich isotherms at 20, 25, 30, and 35 °C

Table 3 Parameters experimentally determined by Langmuir equations

	Temperature (°C)			
	20	25	30	35
Equation	$C_e/q_e = 0.048C_e + 2.207$	$C_e/q_e = 0.057C_e + 2.196$	$C_e/q_e = 0.071C_e + 2.006$	$C_e/q_e = 0.0628C_e + 2.115$
RL	0.455	0.411	0.339	0.379
q_o (mg g ⁻¹)	20.833	17.544	14.085	15.924
b (L mg ⁻¹)	0.0217	0.0260	0.0354	0.0297
R ²	0.982	0.993	0.960	0.973

triangular interaction between chitosan, *sec*-butylammonium acetate, and hexavalent chromium VI (Shekhawat et al. 2015).

These values were confirmed by analyzing the Freundlich isotherm (Fig. 8). The optimal temperature yielded the best adsorption results (Table 4).

According to the Freundlich isotherms, the interaction between the *sec*-butylammonium cations, chitosan, and hexavalent chromium strengthens as n increases ($1/n$ decreases). From the logarithmic plot of q versus C_e , the constants K_F and n were determined as 0.875 mg L⁻¹ and 1.610, respectively (Table 4). The regression coefficient was 0.9425 at 30 °C.

Here, the values obtained at 30 and 25 °C are very similar. Therefore, combining the results of the Langmuir and Freundlich models, we chose 25 °C as the optimal intermediate temperature.

Another important factor in adsorption processes is the contact time between the metal and the adsorbent. In this research, the optimal contact time was determined as 1 h, sufficiently long for the system to reach adsorption equilibrium (Shekhawat et al. 2015; Kumar et al. 2012).

Comparing these results with other studies, we can verify the efficiency of the adsorbent used, since an adsorption above 99% was obtained (20.833 mg g⁻¹ at pH 4 during 1 h, using 1.0 g of adsorbent), since

larger amounts of adsorbents were used which directly interfere in the adsorption capacity determination. This can be evidenced when taking into consideration the studies by Sargin et al. (2012), which obtained a chromium absorption of 67.10% by using chitosan microcapsules from pollen of three common, wind-pollinated plants (*Acer negundo*, *Cupressus sempervirens* and *Populus nigra*) (70.40 mg g⁻¹ at pH 4.63 during 4 h using 0.1 g of adsorbent) or Kumar et al. 2012, which obtained a chromium absorption of 99.0% by using tetraoctylammonium bromide impregnated chitosan (63.69 mg g⁻¹ at pH 3.5 during 0.5 h using 0.2 g of adsorbent). Another important study was the one by Polowczyk et al. (2016), which obtained a chromium absorption of 99% by using an IRA-400 resin containing both N-methyl-D-glucamine and quaternary ammonium functional groups P(VbNMDG-co-CIVBTA) (677.9 mg g⁻¹ at pH 4.00–5.00 during 24 h using 0.002 g of adsorbent). This corroborates the excellent results we have obtained and also shows the efficiency of the treatment by using chitosan activated with *sec*-butylammonium acetate, a liquid which is easy to be obtained and has a low cost, as shown by Andrade Neto et al. (2016).

It should also be noted that the use of lower quantities of activated chitosan provided an excellent adsorption of chromium and increased adsorption

Table 4 Parameters experimentally determined by Freundlich isotherms

	Temperature (°C)			
	20	25	30	35
Equation	$\text{Log } q_e = 0.781\text{Log}C_e - 0.237$	$\text{Log } q_e = 0.731\text{Log}C_e - 0.204$	$\text{Log } q_e = 0.621\text{Log}C_e - 0.058$	$\text{Log } q_e = 0.693\text{Log}C_e - 0.165$
Kf	0.579	0.625	0.875	0.684
n	1.280	1.368	1.610	1.443
R ²	0.982	0.978	0.922	0.973

capacity as well. This capacity resulted in values above 50 mg g^{-1} when 0.05 g of activated chitosan was used, in preliminary assays.

Conclusion

We demonstrated that IL-treatment of adsorbents promotes the adsorption of heavy metal ions, focusing on the absorption of chromium VI by IL-treated chitosan. We also observed that elevated temperature disfavors the process. We optimized the working temperature ($25 \text{ }^\circ\text{C}$), the reaction time (60 min) and the amount of applied adsorbent (1.00 g). In our preliminary studies, the system reached equilibrium after 1 h (the best reaction time). The adsorption reaction kinetics require investigation in future studies.

Acknowledgments We are grateful to Fundação Educacional Inaciana Padre Sabóia de Medeiros (FED) for supporting this research. We thank Dr. Nivaldo Boralle for the NMR measurements.

References

- Andrade Neto JC, Cabral AS, Oliveira LRD, Torres RB, Morandim-Giannetti AA (2016) Synthesis and characterization of new low-cost ILs based on butylammonium cation and application to lignocellulose hydrolysis. *Carbohydr Polym* 143:279–287
- Borsagli FGLM, Mansur AAP, Chagas P, Oliveira LCA, Mansur HS (2015) *O*-carboxymethyl functionalization of chitosan, complexation and adsorption of Cd (II) and Cr(VI) as heavy metal pollutant ions. *React Funct Polym* 97:37–47
- Dyson PJ, Ellis DJ, Welton T, Parker DG (1999) Arene hydrogenation in a room-temperature ionic liquid using a ruthenium cluster catalyst. *Chem Commun* 1:25–26
- Fan HL, Li L, Zhou SF, Liu YZ (2016) Continuous preparation of Fe_3O_4 nanoparticles combined with surface modification by L-cysteine and their application in heavy metal adsorption. *Ceram Int* 42:4228–4237
- Gomes CS, Piccin JS, Gutterres M (2016) Optimizing adsorption parameters in tannery-dye-containing effluent treatment with leather shaving waste. *Process Saf Environ Prot* 99:98–106
- Gore CT, Omwoma S, Chen W, Song YF (2016). Interweaved LDH/PAN nanocomposite films: Application in the design of effective hexavalent chromium adsorption technology. *Chem Eng J* 284:794–801
- Gupta VK, Nayak A (2012) Cadmium removal and recovery from aqueous solutions by novel adsorbents prepared from orange peel and Fe_2O_3 nanoparticles. *Chem Eng J* 180:81–90
- Gupta VK, Saleh TA (2013) Sorption of pollutants by porous carbon, carbon nanotubes and fullerene—an overview. *Environ Sci Pollut Res* 20:2828–2843
- Gupta VK, Srivastava SK, Mohan D, Sharma S (1997) Design parameters for fixed bed reactors of activated carbon developed from fertilizer waste for the removal of some heavy metal ions. *Waste Manag* 17:517–522
- Gupta VK, Jain R, Nayak A, Agarwal S, Shrivastava M (2011a) Removal of the hazardous dye-tartrazine by photodegradation on titanium dioxide surface. *Mater Sci Eng, C* 31:1062–1067
- Gupta VK, Agarwal S, Saleh TA (2011b) Synthesis and characterization of alumina-coated carbon nanotubes and their application for lead removal. *J Hazard Mater* 185:17–23
- Gupta VK, Ali I, Saleh TA, Nayak A, Agarwal S (2012a) Chemical treatment technologies for waste-water recycling—an overview. *RSC Adv* 2:6380–6388
- Gupta VK, Jain R, Mittal A, Saleh TA, Nayak A, Agarwal S, Sikarwar S (2012b) Photo-catalytic degradation of toxic dye amaranth on TiO_2/UV in aqueous suspensions. *Mater Sci Eng C* 32:12–17
- Gupta VK, Mittal A, Jhare D, Mittal J (2012c) Batch and bulk removal of hazardous colouring agent Rose Bengal by adsorption techniques using bottom ash as adsorbent. *RSC Adv* 2:8381–8389
- Gupta VK, Kumar K, Nayak A, Saleh TA, Barakat MA (2013) Adsorptive removal of dyes from aqueous solution onto carbon nanotubes: a review. *Adv Colloid Interface Sci* 193–194:24–34
- Gupta VK, Nayak A, Agarwal S (2015) Bioadsorbents for remediation of heavy metals: current status and their future prospects. *Environ Eng Res* 20:1–18
- He J, Bardelli F, Gehin A, Silvester E, Charlet L (2016) Novel chitosan goethite bionanocomposite beads for arsenic remediation. *Water Res* 101:1–9
- Jeon C, Holl WH (2003) Chemical modification of chitosan and equilibrium study for mercury ion removal. *Water Res* 37:4770–4780
- Jia X, Gong D, Xu B, Chi Q, Zhang X (2016) Development of a novel, fast, sensitive method for chromium speciation in wastewater based on an organic polymer as solid phase extraction material combined with HPLC–ICP-MS. *Talanta* 147:155–161
- Kahu SS, Shekhawat A, Saravanan D, Jugade RM (2016) Two fold modified chitosan for enhanced adsorption of hexavalent chromium from simulated wastewater and industrial effluents. *Carbohydr Polym* 146:264–273
- Karthikeyan S, Gupta VK, Boopathy R, Titus A, Sekaran G (2012) A new approach for the degradation of high concentration of aromatic amine by heterocatalytic Fenton oxidation: kinetic and spectroscopic studies. *J Mol Liq* 173:153–163
- Kumar ASK, Gupta T, Kakan SS, Kalidhasana S, Rajesh V, Rajesh N (2012) Effective adsorption of hexavalent chromium through a three center (3c) co-operative interaction with an ionic liquid and biopolymer. *J Hazard Mater* 239–240:213–224
- Li L, Li Y, Cao L, Yang C (2015) Enhanced chromium (VI) adsorption using nanosized chitosan fibers tailored by electrospinning. *Carbohydr Polym* 125:206–213
- Luo X, Zhang Z, Zhou P, Liu Y, Ma G, Lei Z (2015) Synergic adsorption of acid blue 80 and heavy metal ions ($\text{Cu}^{2+}/\text{Ni}^{2+}$) onto activated carbon and its mechanisms. *J Ind Eng Chem* 27:164–174

- Ma X, Liu X, Anderson DP, Chang PR (2015) Modification of porous starch for the adsorption of heavy metal ions from aqueous solution. *Food Chem* 181:133–139
- Malekia A, Hayati B, Naghizadeh M, Joo SW (2015) Adsorption of hexavalent chromium by metal organic frameworks from aqueous solution. *J Ind Eng Chem* 28:211–216
- Matouq M, Jildeh N, Qtaishat M, Hindiyeh M, Al Syouf MQ (2015) The adsorption kinetics and modeling for heavy metals removal from wastewater by Moringa pods. *J Environ Chem Eng* 3:775–784
- Mittal A, Mittal J, Malviya A, Gupta VK (2009a) Adsorptive removal of hazardous anionic dye “Congo red” from wastewater using waste materials and recovery by desorption. *J Colloid Interface Sci* 340(2009):16–26
- Mittal A, Kaur D, Malviya A, Mittal J, Gupta VK (2009b) Adsorption studies on the removal of coloring agent phenol red from wastewater using waste materials as adsorbents. *J Colloid Interface Sci* 337:345–354
- Mittal A, Mittal J, Malviya A, Kaur D, Gupta VK (2010a) Decoloration treatment of a hazardous triarylmethane dye, Light Green SF (Yellowish) by waste material adsorbents. *J Colloid Interface Sci* 342:518–527
- Mittal A, Mittal J, Malviya A, Gupta VK (2010b) Removal and recovery of Chrysoidine Y from aqueous solutions by waste materials. *J Colloid Interface Sci* 344:497–507
- Pavia DL, Lampman GM, Kriz GS, Vyvyan JR (2015) Introduction to spectroscopy, 5th edn. Cengage Learning, Washington
- Polowczyk I, Urbano BF, Rivas BL, Bryjak M, Kabay N (2016) Equilibrium and kinetic study of chromium sorption on resins with quaternary ammonium and N-methyl-D-glucamine groups. *Chem Eng J* 284:395–404
- Saleh TA, Gupta VK (2012a) Photo-catalyzed degradation of hazardous dye methyl orange by use of a composite catalyst consisting of multi-walled carbon nanotubes and titanium dioxide. *J Colloid Interface Sci* 371:101–106
- Saleh TA, Gupta VK (2012b) Column with CNT/magnesium oxide composite for lead (II) removal from water. *Environ Sci Pollut Res* 19:1224–1228
- Saleh TA, Gupta VK (2014) Processing methods, characteristics and adsorption behavior of tires derived carbons: a review. *Adv Colloid Interface Sci* 211:93–101
- Sargin I, Kaya M, Arslan G, Baran T, Ceter T (2012) Preparation and characterisation of biodegradable pollen–chitosan microcapsules and its application in heavy metal removal. *Bioresour Technol* 177:1–7
- Shekhawat A, Kahu S, Saravanan D, Jugade R (2015) Synergistic behaviour of ionic liquid impregnated sulphate-crosslinked chitosan towards adsorption of Cr(VI). *Int J Biol Macromol* 80:615–626
- Shinde RN, Pandey AK, Acharya R, Guin R, Das SK, Rajurkar NS, Pujari PK (2013) Chitosan-transition metal ions complexes for selective arsenic(V) preconcentration. *Water Res* 47:3497–3506
- Silverstein RM, Webster F, Kiemle D (2005) Spectrometric identification of organic compounds, 7th edn. Wiley, New York
- Tan C, Zeyu Z, Sai X, Hongtao W, Wenjing L (2015) Adsorption behavior comparison of trivalent and hexavalent chromium on biochar derived from municipal sludge. *Bioresour Technol* 190:388–394
- Wu Y, Fan Y, Zhang M, Ming Z, Yang S, Arkin A, Fang P (2016) Functionalized agricultural biomass as a low-cost adsorbent, utilization of rice straw incorporated with amine groups for the adsorption of Cr(VI) and Ni(II) from single and binary systems. *Bio Chem Eng J* 105:27–35
- Xiang B, Fan W, Yi X, Wang Z, Gao F, Li Y, Gu H (2016) Dithiocarbamate-modified starch derivatives with high heavy metal adsorption performance. *Carbohydr Polym* 136:30–37
- Xiao Q, Sun Y, Zhang J, Li Q (2015) Size-dependent of chromium (VI) adsorption on nano α -Fe₂O₃ surface. *Appl Surf Sci* 356:18–23
- Xiao K, Xu F, Jiang L, Duan N, Zheng S (2016) Resin oxidation phenomenon and its influence factor during chromium (VI) removal from wastewater using gel-type anion exchangers. *Chem Eng J* 283:1349–1356
- Yang R, Li H, Huang M, Yang H, Li A (2016) A review on chitosan-based flocculants and their applications in water treatment. *Water Res* 95:59–89
- Yue ZB, Li Q, Li C, Chen TH, Wang J (2015) Component analysis and heavy metal adsorption ability of extracellular polymeric substances (EPS) from sulfate reducing bacteria. *Bioresour Technol* 194:399–402
- Zeng L, Chen Y, Zhang Q, Guo X, Peng Y, Xiao H, Chen X, Luo J (2015) Adsorption of Cd(II), Cu(II) and Ni(II) ions by cross-linking chitosan/rectorite nano-hybrid composite microspheres. *Carbohydr Polym* 130:333–343
- Zhou J, Wang Y, Wang J, Qiao W, Long D, Ling L (2016) Effective removal of hexavalent chromium from aqueous solutions by adsorption on mesoporous carbon microspheres. *J Colloid Interface Sci* 462:200–207